# Experimental and numerical study of Advanced Transfer Path Analysis applied to a box prototype

Àngels Aragonès[2], J. Poblet-Puig[*2], Kevin Arcas[1], Pere Vicens Rodríguez[1], F.X. Magrans[†1,2] and A. Rodríguez-Ferran[‡2]

[2]Laboratori de Càlcul Numèric, E.T.S. d'Enginyers de Camins, Canals i Ports de Barcelona, Universitat Politècnica de Catalunya
[1]Ingeniería para el Control del Ruido

May 3, 2018

**Abstract**

Advanced Transfer Path Analysis (ATPA) is a technique that allows the characterisation of vibroacoustic systems not only from the point of view of contributions but also topologically by means of the path concept. Some of the aspects addressed in the current research such as the proper characterisation of the less contributing paths remained not proven. ATPA is applied to a cuboid-shaped box. The simplicity of this vibroacoustic system helps to make a detailed analysis of the ATPA method in a more controlled environment than in situ measurements in trains, wind turbines or other mechanical systems with complex geometry, big dimensions and movement. At the same time, a numerical model (based on finite elements) of the box is developed. The agreement between the experimental measurements and the numerical results is good. The numerical model is used in order to perform tests that cannot be accomplished in practise. The results are helpful in order to verify hypotheses, provide recommendations for the testing procedures and study some aspects of ATPA such as the reconstruction of operational signals by means of direct transfer functions or to quantify and understand which are the transmission mechanisms in the box.

**Keywords:** ATPA, TPA, path, subsystem, transfer, finite element

[*]correspondence: UPC, Campus Nord B1, Jordi Girona 1, E-08034 Barcelona, Spain, e-mail: jordi.poblet@upc.edu

[†]correspondence: Berruguete 52, Vila Olímpica (Vall d'Hebron), E-08035 Barcelona, Spain, e-mail: fxmagrans@icrsl.com

[‡]correspondence: UPC, Campus Nord C2, Jordi Girona 1, E-08034 Barcelona, Spain, e-mail: antonio.rodriguez-ferran@upc.edu

# 1 Introduction

A major concern when dealing with vibroacoustic systems is to understand how the vibration and noise are transmitted and distributed. A common way to acquire this knowledge is through the path concept. In a network of interconnected nodes we understand that there exists a path between the node $i$ and the node $j$ simply if they are connected. In a vibroacoustic system the nodes are control points, and signals (vibrations or acoustic pressure) are used in order to identify and study the paths. It is not the same a path from $i$ to $j$ as a contribution from $i$ to $j$. A contribution describes the amount of signal that arrives at $j$ due to an excitation on $i$. But this signal can be transmitted through any path from $i$ to $j$ (regardless of the existence of a direct path between $i$ and $j$). So, the contributions are descriptions of the inputs and the outputs while paths are a description of the system topology. One formal definition of 'path' can be found in [1]. More recently, it was shown in [2] that the solution of a mechanical problem can be expressed in terms of paths. This can be used at both numerical modelling and experimental levels. An application example is to characterise the transmission of vibration and noise from the engine to the passengers cavity or other parts of a car. It is usually generated at the wheels, engine, exhaust and travels through the chassis, axes and insulating layers to the passenger compartment.

The final goal is always to characterise the response of each subsystem (measured in terms of the acceleration of a vibrating element or the acoustic pressure in a zone of interest) caused by a specific excitation. A large amount of experimental methods have been developed during the past decades [3]. We can distinguish, in a quite general classification: Transfer Path Analysis (TPA [4]) and Advanced TPA (ATPA [5, 6] or also Force contribution analysis [7]). The main difference between the methods grouped under the name TPA and the name ATPA is that traditional TPA characterises only the source contributions from the inputs to some receivers. It is done by combining operational signals (measured while the equipment is working) with transfer functions (frequency response functions, FRF) measured on the empty passive structure where the equipment is installed. For example, the transfer functions can be measured on a car chassis prior to the engine installation. This chassis is uncoupled from the engine and passive in the sense that it only acts as transmitter of vibrations that are generated elsewhere. ATPA, as the in-situ TPA procedure [8, 9], does not require any disassembly of the structure. It characterises furthermore the topology of the mechanical system and thus, the paths and their contribution to any receiver. TPA measures global transfer functions between subsystems while ATPA measures the direct transfer functions. Direct transfer functions provide a more useful information on the system behaviour. Another feature of ATPA is that, contrary to TPA, the measurement of the excitation force is not required which is indeed an advantage. Both ATPA and TPA are adequate if one can act on the exciting forces to control and reduce them. This means that a redesign of the vibroacoustic system acts on the exciting force in order to improve the response in terms of noise emission or vibration levels. However only with ATPA it is possible to quantify the contributions of a passive system (like the interior panels of a train coach or of a vehicle ) and with this information decide which part of this system needs to be modified in order to reduce the noise measured in the receiver position (the redesign acts on the system

itself).

If the studied system is understood as a black box with $n$ inputs and $m$ outputs interconnected through the box, TPA and ATPA can predict which is the contribution of each input to each output. This means that both methods are able to decompose the output signal into contributions coming from every input signal. However, TPA is unable to describe how the input and outputs are connected. ATPA is able to characterise, in addition, how the input and output signals are connected inside the black box, discover which is the intrinsic structure of the mechanical system, which and how are the paths. For this reason when a detailed analysis of the mechanical system is needed, the use of ATPA is helpful.

## 1.1 Goals of the research

This work deals with the application of the ATPA method to a simple laboratory prototype. This is a cuboid-shaped box with an air cavity inside. A major control on the laboratory measurements is possible due to the simplicity of the prototype. This allows a more detailed analysis. It also opens some unusual options for the analysis of the method that are not possible in more complex mechanical systems such as a car or a train coach. TPA and ATPA methods have several common limitations in practice such as: difficulty in the access to the desired control points, limit in the number of sensors to be used, large time required to make the installation of the measurement setup, difficulty in the repetition of tests (i.e. time to measure in a building, car or train is often limited), etc. All these drawbacks are non-existent in the box prototype because it is available at the lab, sensors can therefore be placed without problems (the box is lightweight and it can be handled and moved without external machinery).

A numerical model of the box is also developed. The degree of uncertainty of the experiment is more controlled than usual. Consequently a better agreement between the numerical model and the experimental data can be obtained. Once calibrated, the numerical model will allow for a faster execution of virtual experiments, the possibility of doing parametric analyses or a more visual representation of the results. In other words, to analyse and gain understanding of aspects that are very difficult to visualise and control in the laboratory or in situ test such as: automatic identification of the subsystems, optimisation of the sensor position inside each subsystem, combination of more than one sensor per subsystem, study the influence of the excitation type (point force, rain-on-the roof, acoustic wave, etc.) and the spectrum of the excitation.

The application of the ATPA method in a vibroacoustic mechanical system as well as the comparison with a numerical model have not been reported before.

## 1.2 Contributions of the research

In addition to the application of ATPA to a vibroacoustic problem as the box with cavity inside, the main contributions of the research and results shown here are:

1. To be able to compute any transmission path with ATPA and show that it properly characterises the paths with small contributions (not only the main contributors). This is important because after a redesign oriented to suppress

the most contributing paths, these other still remain and are the ones that define the response of the modified system.

2. To verify that two methods of estimation of the direct transfer functions provide equivalent results. One of the methods is used in laboratory and in situ measurements and the other is based on the definition of direct transfer.

3. Numerically prove that the error in the reconstruction of a signal by means of the direct transfer functions can be estimated by the direct field (displacement or pressure field when all the control points are blocked).

4. Study the influence of the excitation type in order to reconstruct operational signals.

### 1.3 Precedents of ATPA

The theoretical bases of the ATPA method were presented in [1]. The framework of the global and direct transfer matrices as well as their relationship were defined. Later some applications were done, based on theoretical models and experimental measurements of simple systems. The method presented in [1] and also referred to as Global Transfer Direct Transfer (GTDT) was considered in [10] to theoretically study a mechanical system made of masses and springs. Later in [6], GTDT was similarly applied to a real mechanical device composed of a mass on four springs. The agreement between computed and measured transmissibilities was good. There are other techniques that share with GTDT the determination of direct transmissibilities with an artificial excitation and posterior use of them to simulate the operational response of the system, see for example [11]. The establishment of GTDT as an experimental method for the analysis of mechanical systems was done in [5], where the specification of the experimental procedure and main steps were explained. The name given to the measurement procedure based on GTDT was ATPA. It was included in the review of TPA methods [3] where some of the similitudes and differences with the other available techniques can be seen.

In the remainder of the paper, the ATPA method is reviewed in Section 2.1. The laboratory setup and the numerical model are described in Sections 2.2 and 2.3 respectively. The results are shown in Section 3 before the conclusions of Section 4.

## 2 Methodology

### 2.1 The ATPA method

The ATPA method is based on the theory of transfer matrices presented in [1]. The coefficients of the global transfer matrix $\mathbf{T}^G$ (or also 'GT') are defined as

$$\mathbf{T}^G_{ij} = \frac{x_j}{x_i} \tag{1}$$

where $x_j$ is the signal at node $j$ whilst an excitation is applied only at node $i$. This can be any measure that characterises somehow the behaviour of the mechanical system. Typically $x_j$ is an acceleration, a rotation acceleration or a pressure.

A very important aspect in an ATPA is the proper definition of the subsystems: sets of degrees of freedom represented by only one sensor with signal $x_j$ (i.e. an accelerometer that must be a representative measure of the movement for the whole subsystem). The final quality of the results highly depends on this aspect. In practise one sensor is used in order to characterise each subsystem. The proper definition of subsystems is a common requirement of many different experimental or modelling techniques, see for example [12, 13]. This can also be done by means of the path concept and transfer matrices as described in [14]. The subsystems can be not only representative of physical regions but of mechanical behaviour (bending, in-plane vibrations, etc). Their definition needs an a posteriori verification because it must be consistent with the ATPA results. At the end, the system can be topologically understood as a network where a set of nodes or control points are interconnected by means of transfer functions.

The global transfer is the usual situation found when there is an excitation, a receiver (microphone or accelerometer) and the received signal is due to all possible transmission paths. This is the case of the car in Fig. 1(a) where the sound pressure level (SPL) in the micro is due to the vibration of all the car subsystems (and direct sound from the excited system to the microphone).

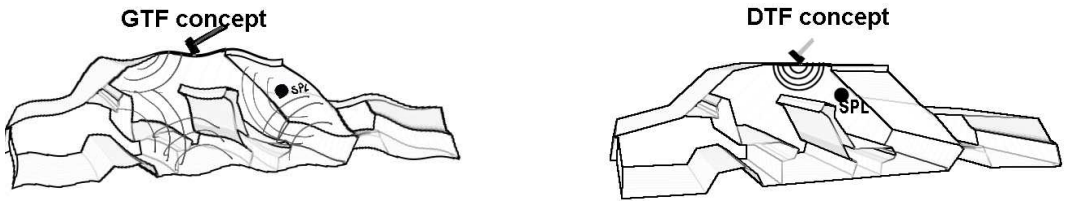


(a) (b)

Figure 1: Sketch of the global transfer and direct transfer concepts applied to an ATPA test of a car. The excitation is a hammer impact applied on a car subsystem. The target is the sound pressure level (SPL) on a micro placed inside the passengers cabin. The two variants are: (a) Global transfer, no subsystem is blocked and all possible paths from the excited and non-excited subsystems to the target are possible. The target signal has contributions from all subsystems passing through all the paths; (b) Direct transfer, where only one transmission path linking the excited subsystem and the target microphone is allowed. Figure reproduced from [5].

A different situation is when all the subsystems are blocked (except the one which is excited and the one which contains the receiver) and the transmission from the excitation to the receiver can only be done through a single path. This is rarely found in real life and can only be reproduced with many difficulties under laboratory conditions. An example is the strip method [15], see for example Fig. 1(b). This is a car where only the excited subsystem is able to vibrate and radiate sound into the passenger compartment. This is an artificial (and difficult to reproduce in the laboratory) situation. All the components of the car must be covered (blocked) and only be uncovered one-by-one in order to generate a single transmission path between the excited subsystem and the receiver.

Paths are characterised by means of the direct transfer matrix $\mathbf{T}^D$ (or 'DT'). Any of the nodes can be considered as transmitter ($i$), receptor ($j$) or both at the same time. The coefficient $\mathbf{T}^D_{ij}$ has information about the path between the nodes $i$ and $j$ and is defined as

$$\mathbf{T}^D_{ij} = \frac{x_j}{x_i} \tag{2}$$

with all the nodes other than $i$ and $j$ blocked. The direct transfer can also be defined from any of the nodes to an external target point $T$ where some output of interest is defined and controlled

$$\mathbf{T}^D_{iT} = \frac{p_T}{x_i} \tag{3}$$

In that case $p_T$ can be the pressure at the target point $T$ when an excitation is applied at $i$ and all the nodes $j \neq i$ are blocked. Even if this situation could be reproduced and all the paths characterised one by one, it would be time-consuming and costly. ATPA overcomes this difficulty.

At this point, we can see that global transfers are related with contributions (quantitative) while direct transfers are related with the path concept (qualitative and also quantitative). The direct transfers provide information on how and through which subsystems the vibrations and sound are transmitted. Global transfers can be more easily measured, while direct transfers require more post-processing.

In the ATPA method, the mechanical system is tested under the condition of Fig. 1(a) where global transfer can be measured. It can be formulated as [1, 16]

$$p_T = \sum_{i=1}^{N} x_i \mathbf{T}^D_{iT} + p^e_T \tag{4}$$

where $p_T$ is a signal in the target (i.e. pressure in a microphone placed inside the passenger's compartment of a car), $x_i$ is the measured signal in subsystem $i$ (i.e. acceleration of a vibrating panel), $\mathbf{T}^D_{iT}$ are the direct transfers between subsystem $i$ and the target and $N$ is the number of subsystems in which the mechanical system has been divided. $p^e_T$ is the direct field of the signal that arrives at $T$ due to an external excitation when all the $N$ nodes are blocked.

In addition, a relationship between the global transfer defined in Eq. (1) and the direct transfer defined in Eq. (3) can be obtained [1]

$$\sum_{j=1}^{N} \mathbf{T}^G_{ij} \mathbf{T}^D_{jT} = \mathbf{T}^G_{iT} \text{ for } i = 1, 2, \ldots, N \tag{5}$$

The characterisation of the paths is then reduced to the mathematical problem of determining the coefficients $\mathbf{T}^D_{iT}$. This can be done, for example, by means of the solution of the linear system of just $N$ equations like Eq. (5) (for the case of exactly $N$ executions of the experiment).

In ATPA, following the definition of $\mathbf{T}^G$, a different subsystem is excited at every execution of the experiment. This guarantees the linear independence of the $N$ equations and the linear independence of the signal sensors measurements at every excitation case of the experiment (understood as statistical information). In other

| Plate | Thickness $h$ [m] |
|---|---|
| Top | $8 \times 10^{-3}$ |
| Front | $1 \times 10^{-2}$ |
| Back | $1 \times 10^{-2}$ |
| Left | $1 \times 10^{-2}$ |
| Right | $8 \times 10^{-3}$ |

Table 1: Box plate thicknesses

words, more different responses of the mechanical system are included in its characterisation and the information is more representative. In addition, the understanding of the coefficients in Eq. (5) as direct transfers, allows the experimental procedure to be split and use a reduced number of channels at the same time if needed. There is no need to measure all $N$ subsystems simultaneously which is an advantage in complex and large systems where the number of subsystems is larger than the number of available channels. Even if it is more comfortable to perform all the measures at the same time, the possibility of splitting this acquisition of data is always interesting.

The ATPA test has two different variants: coherent and energetic. In the coherent case, the contributions are taken into account in modulus and phase, in the strict sense of Eq. (4). On the contrary, the energetic variant, deals with scalar outputs that are representative of the subsystem energy. All the results and analysis presented here are based on the coherent version of the ATPA method. This means that all quantities are complex numbers and the reconstruction of signals in Eq. (4) must account for real and imaginary parts. We verified that all the results and comparisons in Section 3 are consistent in modulus and phase. For the sake of clarity, only the modulus is shown in the figures.

## 2.2 Description of the experimental setup

The prototype of the cuboid-shaped box is shown in Fig. 2. It is made of methacrylate with dimensions $L_x = 0.534$ m, $L_y = 0.426$ m and $L_z = 0.586$ m. In general, it is designed in order to be complex enough to test the ATPA method but also as simple as possible to allow a proper numerical modelling with as few uncertainties as possible. For example, in order to satisfy the first goal, the three box dimensions and also the face thickness (see Table 1) are different, to try to decouple as much as possible the vibration and resonances of the rectangular faces. And in order to reduce the uncertainties, all the junctions at the edges are made as homogeneous as possible. The two methacrylate plates are glued to each other at each edge. The bottom part is made of multiple thin steel plates separated by layers of rubber damping material. The solid steel layers provide the stiffness and the mass while the rubber between them ensures large damping. Consequently, its vibration can be neglected when compared with the vibration of the other faces. It also includes several latches that are used to detach and fix the methacrylate part (the box needs to be accessible in order to place the microphones inside).

Twenty control points are considered. Four of them are placed at the centre of

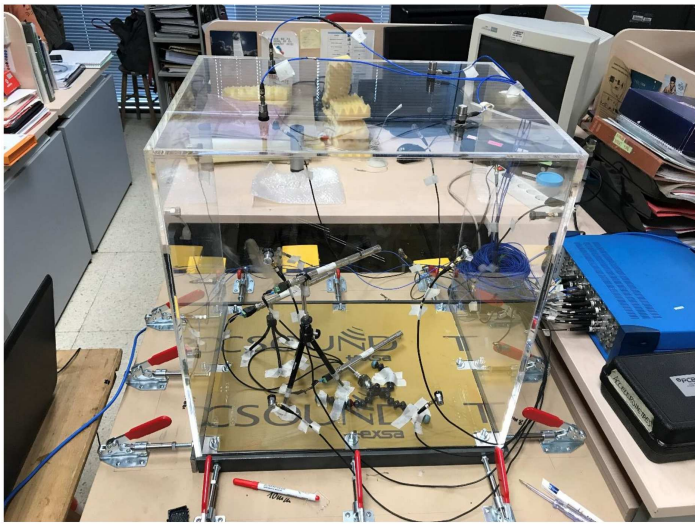

Figure 2: Experimental setup including the box, twenty accelerometers (four per face) and three microphones inside.

each quarter in the five vibrating faces. The notation and position of them is shown in Fig. 3. An accelerometer is placed at each of these points. At the same time, the excitation is applied also there by means of a hammer impact (in general) or a fixed shaker (only in the calibration phase discussed in Section A.2).

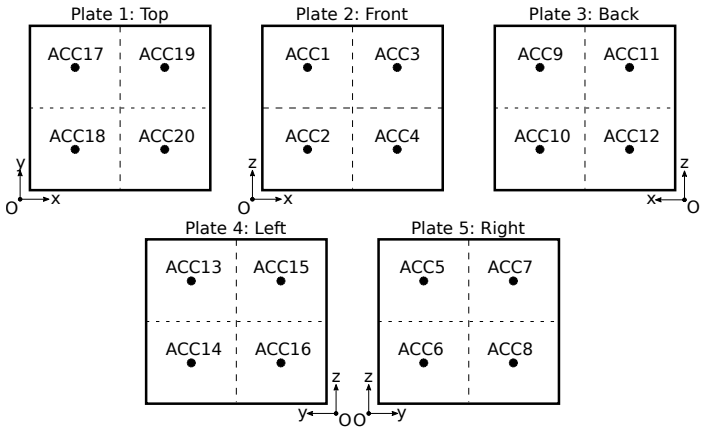


Figure 3: Sketch with the distribution of the accelerometers.

On the one hand, some of the measured data can be unreliable below 100 Hz. The reasons are several: the foam supports of the rectangular plate as commented above (modify the low frequency modes); the cases where the excitation is done by means of the shaker (it is difficult to induce vibrations when rigid-body motion modes are present); the existence of background noise and vibrations at very low frequencies. On the other hand, the material of the hammer impact zone and the impact velocity limit the validity of experimental data to frequencies below 2000 Hz. So, in order to avoid the use of unreliable data we preferred to keep in the safe side and limit the frequency range of the study from 100 Hz to 2000 Hz.

## 2.3 Description of the numerical model

A virtual setup for the experimental mechanical system described in Section 2.2 is developed. It is based on the finite element method (FEM) by means of the software Code-Aster [17].

The box is modelled by means of triangular shell elements that use DKT formulation [18] to describe the bending behaviour. The nodes in the lower contour of the box are blocked (null displacements and rotations). The material behaviour is linear elastic with hysteretic damping. Perpendicular point and surface forces can be applied on each face. The coupled vibroacoustic problem in the frequency domain is considered. Only the air cavity inside the box is included in the model. The effect of the radiation losses and the air surrounding the box is neglected which is a common assumption in the modelling of this type of vibro-acoustic systems.

Code-Aster [17] is used to solve a single problem (i.e. compute displacement and pressure field due to a point force in a list of given frequencies). However, in order to reproduce all the process of the ATPA method, a script system is required due to the large number of simulations involved. As it will be detailed below in Section 3, point forces need to be applied at each control point and boundary conditions modified sometimes at every simulation. For this reason a systematised procedure is required.

The size of structural elements has been determined by means of a convergence test and set to $2 \times 10^{-2}$ m. The size of acoustical elements has been set to obtain at least 34 elements per wavelength in every 100 Hz frequency band. This is a balance between accuracy and computational costs. The use of variable finite element size in the acoustic part of the problem requires to refine the mesh at several frequencies. This is done as a task inside the frequency loop of the script system. The simulation is split in user-defined frequency-bands and the remeshing is done for each of these steps. In addition, the value of the frequency-dependent parameters is updated.

The mechanical properties considered in the FEM model for the methacrylate are shown in Table 2. The procedure that leads to these values is described in Appendix A.

| Material | $\rho_v$ (kg/m$^3$) | $\nu$ | $E$ (Pa) | $\eta$ |
|---|---|---|---|---|
| methacrylate | 1153.2 | 0.45 | $4.3 \cdot 10^9$ | $0.07 + \frac{1}{\omega}$ |

Table 2: Mechanical properties of the methacrylate ($\rho_v$ is the volumetric density, $\nu$ is the Poisson's ratio, $E$ is the Young modulus and $\eta$ is the hysteretic damping coefficient).

# 3 Results

The most meaningful results obtained by means of the box analysis are reported here. They are organised in four different sections. Section 3.1 mainly shows the efficiency of the ATPA method for characterising all the transmission paths and how the same direct transfers are obtained by means of different procedures. Section 3.2 analyses the influence of the imprecisions in the application of point forces, which is one of

the key aspects of ATPA. Another very important aspect, the use of direct transfers in order to characterise the operational state, is studied in Section 3.3. Finally, the transmission between opposite faces illustrates some other features of the method in Section 3.4.

In all the results shown here a variable number of sensors per face have been considered (one, two, three or four). This leads to very similar results in all the cases, which means that for the box, each face behaves like a subsystem and one accelerometer is enough. It is well known that in structures composed of rectangular plates (for example: L-shaped, T-shaped, X-shaped junctions, see [13]) each rectangular part acts as a subsystem and the junction makes it difficult to spread the vibration energy in the excited plate to the other plates. At the low frequency range the modes of vibration tend to exhibit much larger displacements in one part than in the others (it is like local resonances). At high frequencies, the vibration is more or less uniform (especially if several frequencies are averaged) and we can distinguish different energy levels in every rectangular plate. So, for this type of structures the behaviour is quite binary: vibrate or not. In this situation ATPA needs information of one control point of the subsystem in order to properly characterise the response and the topology.

This can be different in more complex mechanical systems where the definition of subsystems is not so clear. In that situation the use of a more dense network of control points can be mandatory. All these is related with the proper identification of the subsystems. But in any case, the direct transfer function between two points is not depending on the number of sensors considered. $\mathbf{T}^D$ is an intrinsic property of the system. The figures show here the case of four sensors per face, which is almost equivalent to the others. Only the result in Fig. 8 are included to illustrate the unvariability of transfer functions due to the addition of other control points.

## 3.1 Computation of the direct transfer matrix $\mathbf{T}^D$

The direct transfer matrix $\mathbf{T}^D$ defined in Eq. (3) is usually computed as a post-process of the global transfer matrix $\mathbf{T}^G$ as described in Eq. (5). The reason is that the coefficients of $\mathbf{T}^G$ can be directly obtained as measurement output while it is difficult and time-consuming to perform a direct measurement of the $\mathbf{T}^D$ coefficients. Moreover, imposing the boundary conditions would imply a modification of the system. So, it is not clear that in most of the cases this procedure could be done.

To deal with a numerical model helps in order to overcome these difficulties because it is easier and faster to handle the boundary conditions and virtually perform repetitive experiments. Blocking all the subsystems except two is more easily done in a computational model than in a laboratory experiment.

Two procedures to compute $\mathbf{T}^D$ are considered:

1. *'Mimics the experiment (labelled 'from GT'):* Excitation of the box at points $i = 1, 2, \ldots, N$. Each excitation applied to a node $i$ provides a row of the matrix $\mathbf{T}^G$ and the coefficient $\mathbf{T}^G_{iT}$. The direct transfer matrix can be obtained from Eq. (5). Afterwards, $N$ simulations per frequency are required in order to generate the linear system of equations (4).

2. *'Apply the definition of* $\mathbf{T}^D$ *(labelled 'from definition')':* Excitation of the box at points $i$ with all the other nodes $j \neq i$ blocked. With this simulation type, the coefficients $\mathbf{T}^D_{iT}$ are obtained. This situation is difficult to consider in the laboratory because it requires time to block all the paths except the one that is studied (from the excitation point $i$ to the target $T$). Most probably, this procedure cannot be done experimentally because the original system would be altered.

Fig. 4 shows two representative computations of a direct transfer matrix coefficient: Fig. 4(a) for the transmission from an excited point to one of the micros inside the cavity and Fig. 4(b) for points placed on the box structure. In both cases ('from GT' and 'from definition' ) the values of $\mathbf{T}^D$ obtained by means of the numerical model are almost equivalent in the whole frequency range. This is the case for all the direct transfer functions to the microphones and between accelerometers as it can be seen in Fig. 4(a).

However, some difference has sporadically been found as it can be seen in Fig. 4(b) around 300 Hz. The very few times that this is observed, coincides with the peaks of the curves. They are associated at some of the system resonances. Numerical models can suffer from small eigenfrequency shifts and it is know that numerical error can be larger around the eigenfrequencies. Also matrices can be ill-conditioned which help in the propagation of possible numerical errors. Both methods to compute $\mathbf{T}^D$ use a system with different spectra (due to the modified boundary conditions). So, it is logical to expect some small difference, especially for poorly damped systems. In any case, the agreement between curves that have been found is in general very accurate.

The experimental curve is obtained from the laboratory measurements and the 'from GT' procedure. This is the only of the two procedures to determine the direct transfer functions presented in Section 3.1 whose application in a real laboratory experiment does not entail very important difficulties and efforts. Otherwise a large amount of different experiments are required if the option 'from definition' is considered. Moreover, the difficulties to impose and modify the boundary conditions are important. The agreement with the computed values is correct.

A similar comment applies for all the 400 structure-to-structure paths (20 sensors on the box acting as transmitter and receivers at the same time) and the 60 structure-to-air paths (20 sensors on the box acting as transmitter and 3 microphones acting as receivers). This is especially relevant because it means that the ATPA method properly characterises not only the dominant paths but also the ones associated with a smaller $\mathbf{T}^D$. Potential redesigns or modifications in order to suppress the dominant transmission paths require the proper characterisation of these less important paths in order to properly predict the new behaviour of the system.

## 3.2 Influence of the error in the position of the hammer impact in the $\mathbf{T}^D$ computation

As explained above in Section 3.1, ATPA requires the excitation of the mechanical system by means of a hammer impact. Moreover, this has to be done multiple times in order to compute the direct transfer matrix $\mathbf{T}^D$ ($N$ times, the same as the number

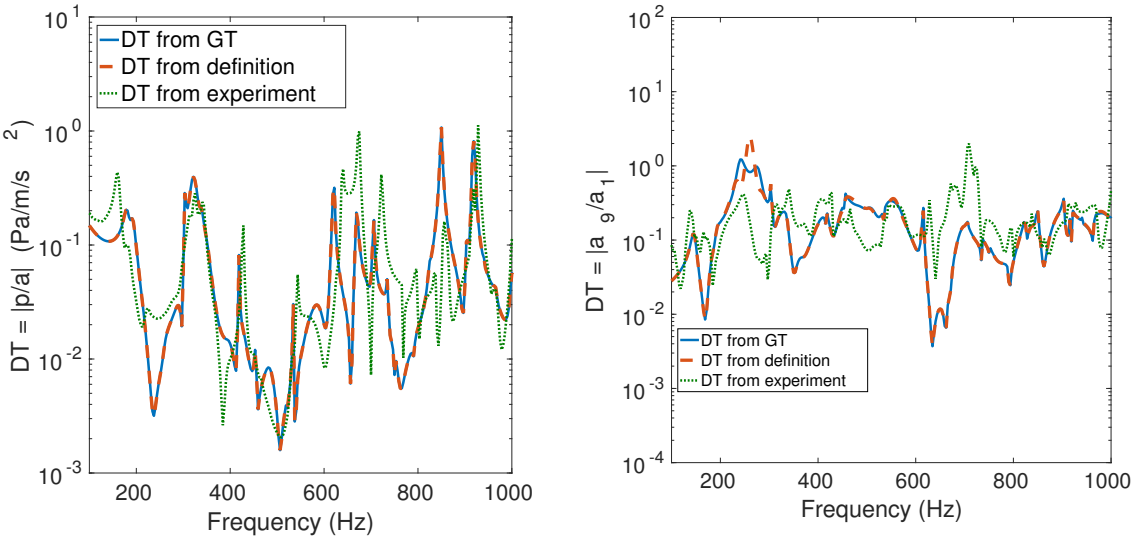


(a) (b)

Figure 4: Direct transfer functions (modulus): (a) from the accelerometer ACC1 to the microphone MIC1, pressure divided by acceleration; (b) from the accelerometer ACC1 to another accelerometer of the box (ACC9). Comparison of experiment results (third curve: 'from experiment') with the two methods of obtaining the direct transfers by means of the numerical model (first and second curves).

of control points). This manual repetitive action is not free of errors and can hinder the reproducibility of the experiment.

The effect of the influence of the precision in the position of the hammer impact on the $\mathbf{T}^D$ computation is checked here by comparing two different scenarios. On the one hand, $\mathbf{T}^D$ is computed by applying the point force at the nominal position (where the sensor or measure point is placed). On the other hand $\mathbf{T}^D$ is computed by applying the point force around this nominal position, approximately, at a distance between 2.5 cm and 4.5 cm. This can be quite representative of deviations in the impacted point in mechanical systems where it is difficult to access and hit with the hammer (i.e. inside a windmill blade).

In the experimental measurement, the hammer impact is not applied at the nominal position. It can be done if adapted acceleration sensors are used (i.e. the accelerometer can be placed on the other side of the plate or it is protected in such a way that is possible to hit directly over the sensor).

An illustrative result is shown in Fig. 5 for the direct transfer between the accelerometer ACC1 and the microphone MIC1. This figure shows three curves: experimental direct transfer, numerical direct transfer with the point force applied at the nominal position where the sensor is placed and numerical direct transfer with the point force applied close to the position where the sensor is placed. The relation between the curves is quite random, depending on the frequency. This illustrates the importance of the excitation type.

More important than the comparison with the experiment is the relation between the two numerical simulations, which shows the influence of the precision in the appli-

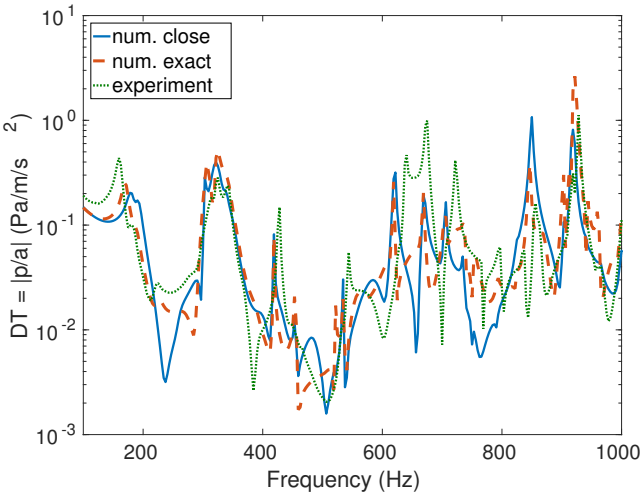


Figure 5: Direct transfer function from the accelerometer ACC1 to the microphone MIC1 (pressure to acceleration ratio $|p/a|$). Comparison of experimental results with the $\mathbf{T}^D$ values obtained by means of the numerical model with a point force applied close to the accelerometer (as it is done with the hammer impact of the experiment) or in the exact point (nominal position).

cation of the point force. To do so, the separation between frequency response curves is measured as

$$e = \frac{\sum_i \left(\psi_{\text{exp}}(f_i) - \psi_{\text{FEM}}(f_i)\right)^2}{\sum_i \left(\psi_{\text{exp}}(f_i)\right)^2} \tag{6}$$

with $\psi_{\text{exp}}$ the experimental measure, $\psi_{\text{FEM}}$ the FEM simulation, $f_i$ the central frequency of the third octave band and the sum is done in all the third octave frequency bands between 125 Hz and 1000 Hz, both included. $\psi_{\text{exp}}$ and $\psi_{\text{FEM}}$ are the result of the frequency average of the signal in the third octave frequency band (i.e. they are the mean response in the band). It is important to note that the outputs are now not averaged in space or excitation cases (only one force position and only one reception point). The results are shown in Fig. 6. In each plot two sets of data are shown. One of them represents the difference considering the third octave bands in the range 160 Hz to 630 Hz. The other considers also the third octave bands equal or below 1000 Hz. It can be seen that while the difference is not very large at the lower frequencies (for most of the paths), it becomes more important at high frequencies. Again it must be taken into account that we are dealing with a linear output and that these differences become less important from the engineering point of view when dealing with outputs expressed in dB scale. There exist a difference between the results in Fig. 6(a) and Fig. 6(b). We have no clear explanation for this and we can also speculate with an small deviation in the micro position. This affects more at high frequencies where the acoustic wavelength becomes shorter and point outputs (non-averaged) can suffer from larger deviations.

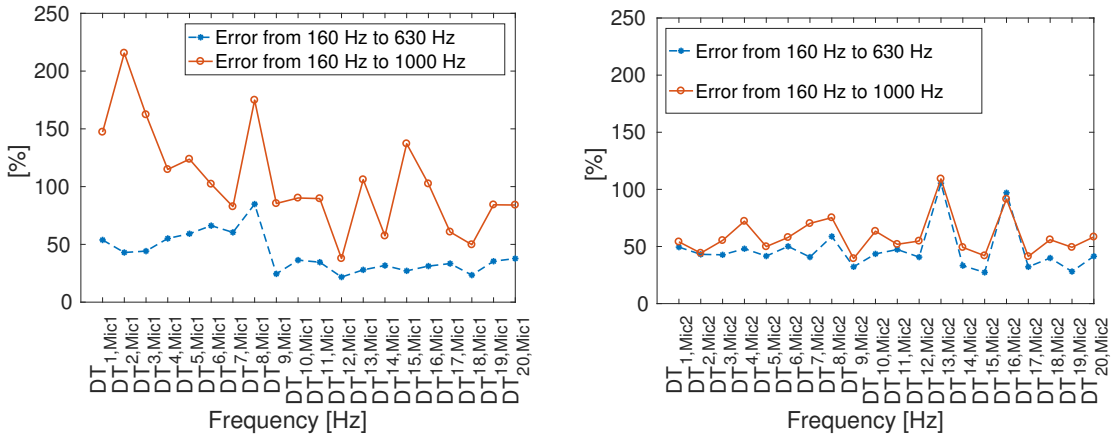


Figure 6: Difference between direct transfer functions when the point force is applied at the nominal position or with an excentricity between 2.5 cm and 4.5 cm. Each curve represents a frequency range where the difference in third octave bands is averaged. All the curves are FEM simulations. Each point in the plot represents the transmission from an accelerometer to a microphone: (a) to MIC1; (b) to MIC2.

## 3.3 Signal reconstruction using the direct transfer matrix

The main output of the ATPA method is the $\mathbf{T}^D$ matrix. It concentrates the information about the transmission paths and can be used to quantify the flow of energy (in the form of vibrations or acoustic pressure) through them. In some sense, the matrix $\mathbf{T}^D$ is a representation of the mechanical system.

However, an excitation type (here the hammer impact) needs to be chosen in order to compute $\mathbf{T}^D$. The value of $\mathbf{T}^D$ is independent of the excitation type. The big question is how the two terms on the right-hand-side of Eq. (4) are balanced. On the one hand, if the signal in the target is properly reconstructed with the sum of contributions through the direct transfers ($\sum_{i=1}^{N} x_i \mathbf{T}^D_{iT}$), this means that the choice of control points is adequate and the system characterisation is excitation-independent. The operational response can be approximated by means of the information condensed in the direct transfer functions. On the other hand, if the second term ($p^e_T$) is important, it means that the signal arriving at the target without passing through the control points (direct field) is relevant and the reconstruction cannot be done by only considering the contributions from the direct transfers. In that situation, a redefinition of the control points is recommended. The new configuration should be able to block the direct field ($p^e_T = 0$). In general, an increase in the density of control points (i.e. putting more sensors on a plate) leads to a decrease of the direct field contribution ($p^e_T \to 0$). Of course, this must be understood as a limit situation because it is difficult to completely block a system for all the frequencies by simply adding control points. The determination of the direct field is more complicated and it would make more tedious the whole process. In general, it is much better if the direct field is small with respect to the paths contribution and consequently it can be neglected.

The purpose of ATPA method is to determine $\mathbf{T}^D$ with a group of excitations that

satisfy: *i)* It is comfortable to apply them to the mechanical system in an instrumented experiment or in situ measure; *ii)* Excite all (or as many as possible) the behaviour types of the mechanical system and generate energy in all the zones (at least in one of the excitations); *iii)* Avoid problems of matrix inversion due to the similarity between all the considered excitations which leads to a poor linear independence of the linear systems to solve, see Eq. (5). Afterwards, the $\mathbf{T}^D$ matrix information is used to predict the real behaviour of the system.

We will refer as 'operational' output as the signal measured or computed when the mechanical system is excited with the real actions (not a test in the laboratory). In that situation the excitation can be almost random or at least different from the hammer impacts. For the case of the methacrylate box an operational state could be generated by means of a loudspeaker moving around the box. For the case of a train wagon, the operational states are the induced vibrations when the train is moving. We will talk also about 'Reconstructed' outputs. This will refer to the response of the system that is computed by means of $\mathbf{T}^D$ and the operational signal of the control points. An expression similar to Eq. (4) is considered. The direct field $p_T^e$ has been in most of the cases neglected. The target output can differ from the pressure in a position. This is specified in every shown simulation.

Fig. 7(a) shows two curves with the absolute value of the pressure in microphone 1 when the point force is applied at ACC1. One of them ('Operational') is the signal directly measured. The other one ('Reconstructed'), is the reconstruction of the pressure in microphone 1 by means of the accelerations in all the control points. $\mathbf{T}^D$ is computed with hammer impacts in the nominal position (the operational behaviour is caused also by the same point force applied at ACC1).

Both pressure curves are exactly the same. This is because the same excitation type is considered in order to compute $\mathbf{T}^D$ and generate the operational state. The same coincidence between curves is observed with the point force applied at any of the control points.

Fig. 7(b) is exactly the same as Fig. 7(a) with the difference that the point forces are not applied at the nominal position where the accelerometer is placed but in the surroundings. The agreement between operational and reconstructed signals is again almost exact.

Some differences can be found if the point force used to generate an operational state of the mechanical system is applied at a position that differs from the ones used to compute the $\mathbf{T}^D$ matrix. Fig. 9 shows this effect.

As mentioned before, four accelerometers per face are considered in all the box results shown here. However, the simulations have also been done with only one, two (side by side and symmetrical with respect to the rectangular face diagonal) and three accelerometers per face. The positions in Fig. 3 are considered and some of the accelerometers are removed. Fig. 8 shows the same signal reconstruction of Fig. 7(b) but using a different number of accelerometers per face. As expected, the results are exactly the same. The transfer function between the accelerometer 1 and the microphone 1 is not modified by adding other accelerometers.

The box has also been excited by means of 88 randomly distributed point forces normal to the face with also random modulus and sign (close to rain-on-the-roof excitation in the sense that point forces are distributed all around the plate but with

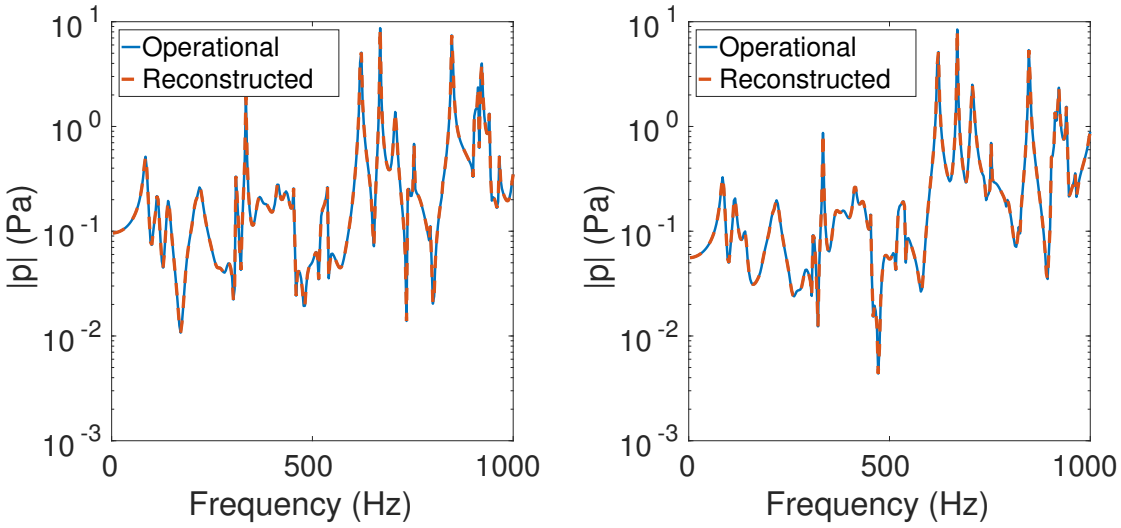


(a) (b)

Figure 7: Signal at microphone MIC1 (absolute value of pressure $|p|$) when a point force is exciting at the position of the accelerometer ACC1. All the curves are FEM simulations. Comparison between operational and reconstructed signals. The two curves are overlapped because the reconstruction is exact. Both the point force considered in the operational state and the point force used to compute the $\mathbf{T}^D$ are placed at: (a) nominal position of the accelerometer; (b) close to accelerometer.

coherent excitation) and a uniform pressure applied at the front face. The results are shown in Fig. 10(a) and Fig. 10(b) respectively. It can be seen that in both cases the differences between operational and reconstructed curves are larger than before but they still have a similar trend and modal distribution. This separation of the curves is due to the different excitation type considered when computing the $\mathbf{T}^D$ and when simulating the operational status.

Fig. 10(b) contains also a third curve. Its goal is to illustrate the effect of the direct field $p_T^e$ in Eq. (4). $p_T^e$ is computed here as the vibration and pressure fields obtained due to the excitation of the mechanical system by means of the operational action but considering the boundary conditions used in the 'from definition' procedure to compute $\mathbf{T}^D$. Here it is the uniform pressure applied at the front face with all the control points blocked. For this reason $p_T^e$ is known as the direct field (signal that arrived when all the control points are blocked, the signal cannot go through alternative paths). We see that the addition of $p_T^e$ to the reconstructed field exactly complements the reconstructed curve in order to fit the 'operational' simulation. This is important and shows that the relationship (4) is exact. $p_T^e$ is usually neglected in the experimental procedures. Among other reasons, because it is very difficult to measure (all control points should be blocked) and because if control points are properly chosen and enough sensors used, $p_T^e$ tends to be small. This numerical simulation shows also that the inherent errors of the ATPA method by neglecting the direct field can be estimated a priori by means of $p_T^e$.

It is shown how the hypothesis of excitation-independence for the direct transfer

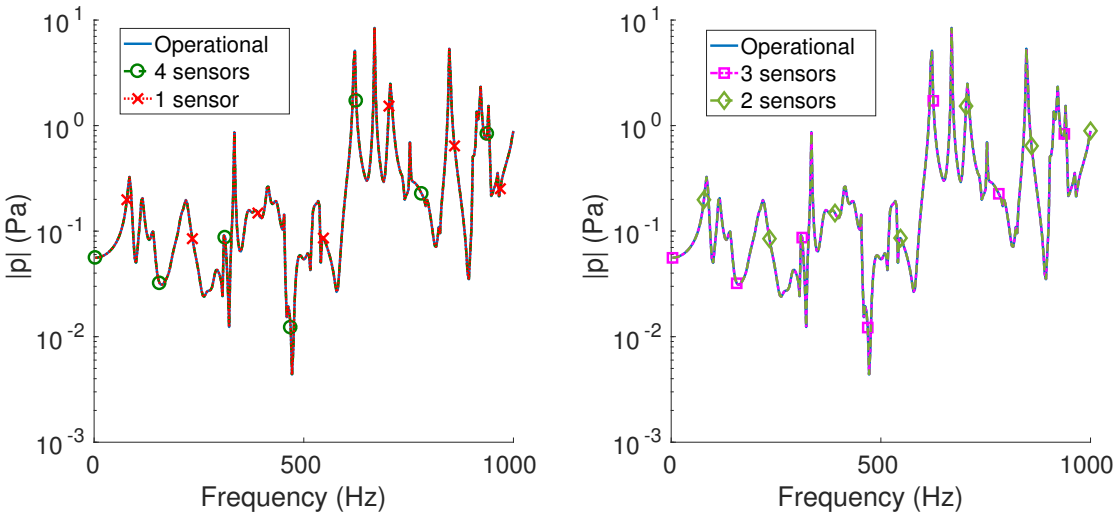


(a) (b)

Figure 8: Signal at microphone MIC1 (absolute value of pressure $|p|$) when a point force is exciting at the position of the accelerometer ACC1. Comparison between operational and reconstructed signals (point force close to accelerometer). All the curves are FEM simulations. Influence of the different number of used sensors per face. Each plot contains three overlapped curves because the reconstruction is exact and the result is not dependent on the number of sensors per face used. Operational signal on both plots is overlapped with the reconstructed signal taking into account: (a) 1 and 4 accelerometers per face; (b) 2 and 3 accelerometers per face.

functions is not completely true and sometimes the direct field is relevant. However, the global trend of the signal is properly reconstructed in spite of the differences at specific frequencies.

## 3.4 Vibration transmission between opposite faces of the box

A particular transmission path is analysed in this section: the vibration transmission between opposite (front and back) faces. This is relevant because there is no direct transmission path between the faces. Moreover, the paths are not only through the structure but also across the air cavity. For these reasons, to properly characterise the transmission caused by a chain of first-order paths is a good challenge in order to test the ATPA method and understand the vibroacoustic response of the box.

A first aspect to be considered is the importance of the cavity paths versus the structural ones. Fig. 11 compares two direct transfers with and without air cavity. In both cases, the values of the function at a specific frequency and the general trend of the curve is very similar. This indicates that the cavity has no important effect on this transmission path and that the coupling air-to-structure is weak. The curve corresponding to the case with cavity shows some more oscillations. This is caused by the increase of modes on the system due to the presence of the cavity. Moreover, the modal density of the cavity is larger than those of the box faces after 500 Hz approximately. At very low frequencies the cavity can produce a more efficient

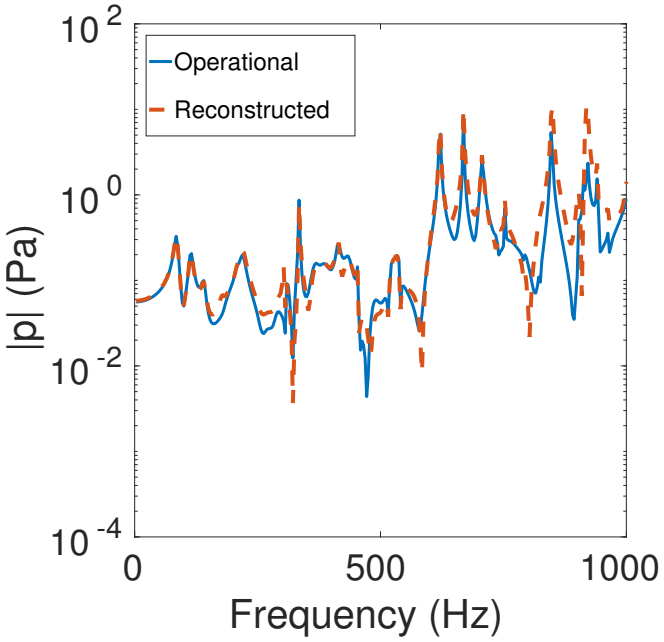


Figure 9: Signal at microphone MIC1 (absolute value of pressure $|p|$) when a point force is exciting at the position of accelerometer ACC1. All the curves are FEM simulations. Comparison between operational and reconstructed signals. The point force excitation is placed close to point ACC1 but $\mathbf{T}^D$ matrix has been computed by means of point forces exciting exactly at points ACCi.

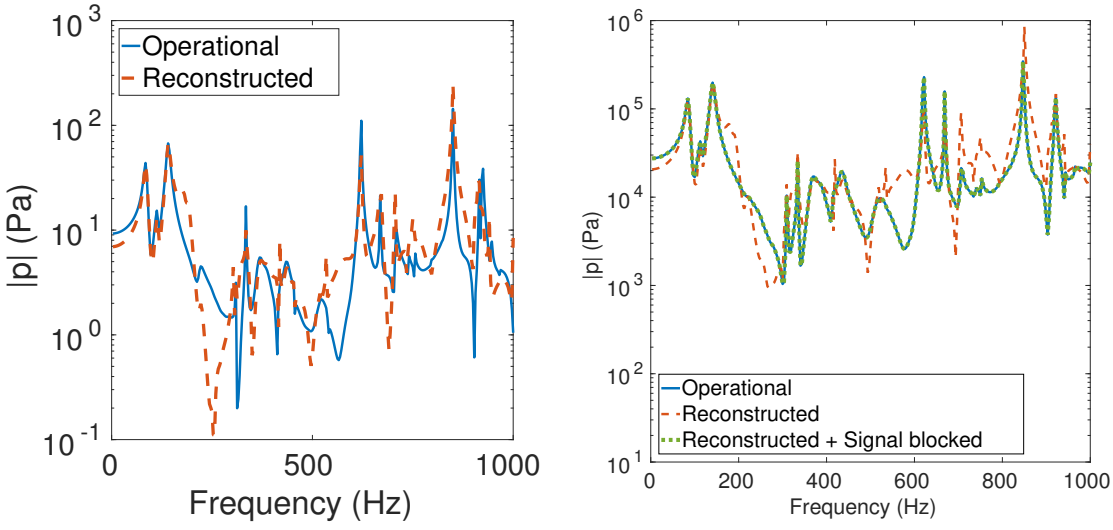


(a) (b)

Figure 10: Signal reconstruction at microphone number 1 (MIC1, absolute value of pressure $|p|$): (a) 88 point forces are randomly distributed all over the front face; (b) the front face is excited with a uniform unitary pressure. All the curves are FEM simulations.

transmission.

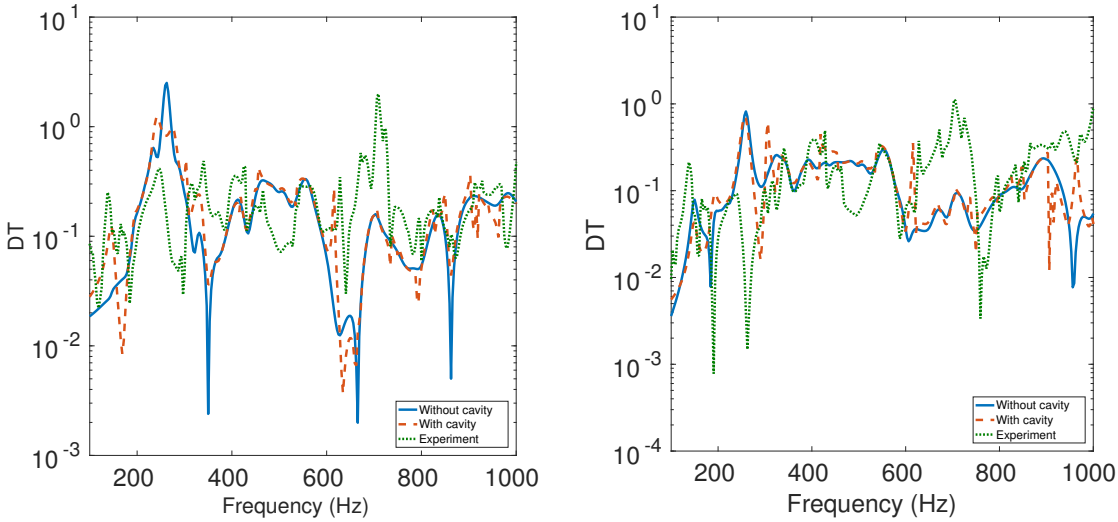


Figure 11: Comparison of the direct transfer between opposite faces of the box with and without air cavity inside: (a) $\mathbf{T}^D_{1,9}$; (b) $\mathbf{T}^D_{1,10}$.

In all the previous results the control points are characterised by the acceleration in the direction normal to the plate (this is chosen among the six degrees of freedom per node in the shell finite element). This is a common option because normal acceleration is measured in a natural way, the vibration is mostly caused by bending and the interaction with the cavity is due to normal displacement. However, the ATPA method deals with degrees of freedom in general and allows dealing with more than one variable per control point. See for example [19] where it is shown how rotations and displacements are relevant for the transmission path analysis of a beam. Fig. 12 shows the comparison for the usual case where only the normal acceleration is considered at each control point and the case where also two rotations are considered. The rotations are the ones with rotation vector in the plane of the plate (i.e. in the control points in the plate with constant X coordinate and acceleration measured in the X direction, the rotations with vectors in the Y and Z directions are considered). These degrees of freedom are chosen as a more detailed an alternative description of the bending response of the plates in the framework of an ATPA analysis. The differences between the two curves are not large and the general trend is the same. This suggests that for the analysis of this box, taking into account the normal acceleration is enough.

It should be noted that experimental measurement of rotations is not straightforward. On the contrary they can be obtained without difficulties from the numerical model which shows again on of the advantages of virtual experiments.

A good option for determining the importance of a transmission path is to compare its direct and global transfer functions. Even if the low-frequency ATPA method works with modulus and phase (complex numbers) and individual paths can cancel each other, the comparison of the absolute value of direct and global transfer functions

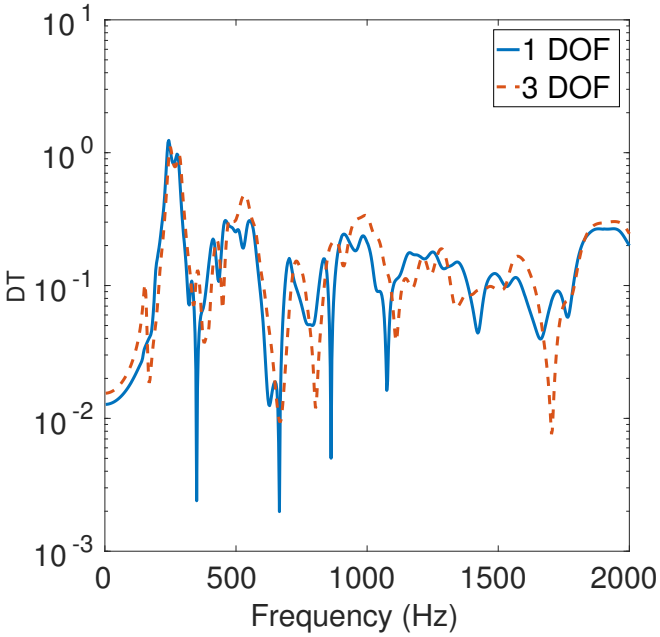


Figure 12: Direct transfer function between two accelerometers computed by means of the FEM: $\mathbf{T}^D_{1,9}$. Comparison between the case when only the normal displacement at each accelerometer (1 DOF: one degree of freedom per control point) is considered or also two rotations are taken into account (3 DOF: three degrees of freedom per control point).

can be a good indicator. A small difference between global and direct transfers means that most of the transmission is done through the path. Fig. 13 shows this comparison for three different transmissions: between opposite faces, between adjacent faces and between sensors placed at the same face. It is clear how the largest difference between frequency response curves is found for the case of opposite faces. This transmission is not done by means of a direct path from face to face, which does not exist, but through indirect paths.

ATPA can be used to discover the topology of a system and determine how the signal is transmitted. To do so, all the direct transmission functions are required. They provide information on the direct connection between control points. Fig. 14 is an example on how by means of the direct transfer matrix the topology of the box can be recovered. It is based on the outputs of the FEM model for the box without air cavity inside at a frequency of 62.5 Hz. Fig. 14(b) is a physical interpretation of the signals, taking into account the geometry of the box and the positions of the accelerometers. The box is unfolded in order to draw it in a single plane with the most important paths in nodes 1 and 4. Fig. 14(a) is a graph map with only the most important transmission paths for all the box. The nodes represent the accelerometers and the arrows the connections. Both figures are just a graphical representation of the direct transfer values of the matrix $\mathbf{T}^D$ shown in Fig. 14(c). There the colours indicate the absolute value of the coefficient.

All the coefficients in the matrix $\mathbf{T}^D$ are ordered (considering their absolute value).

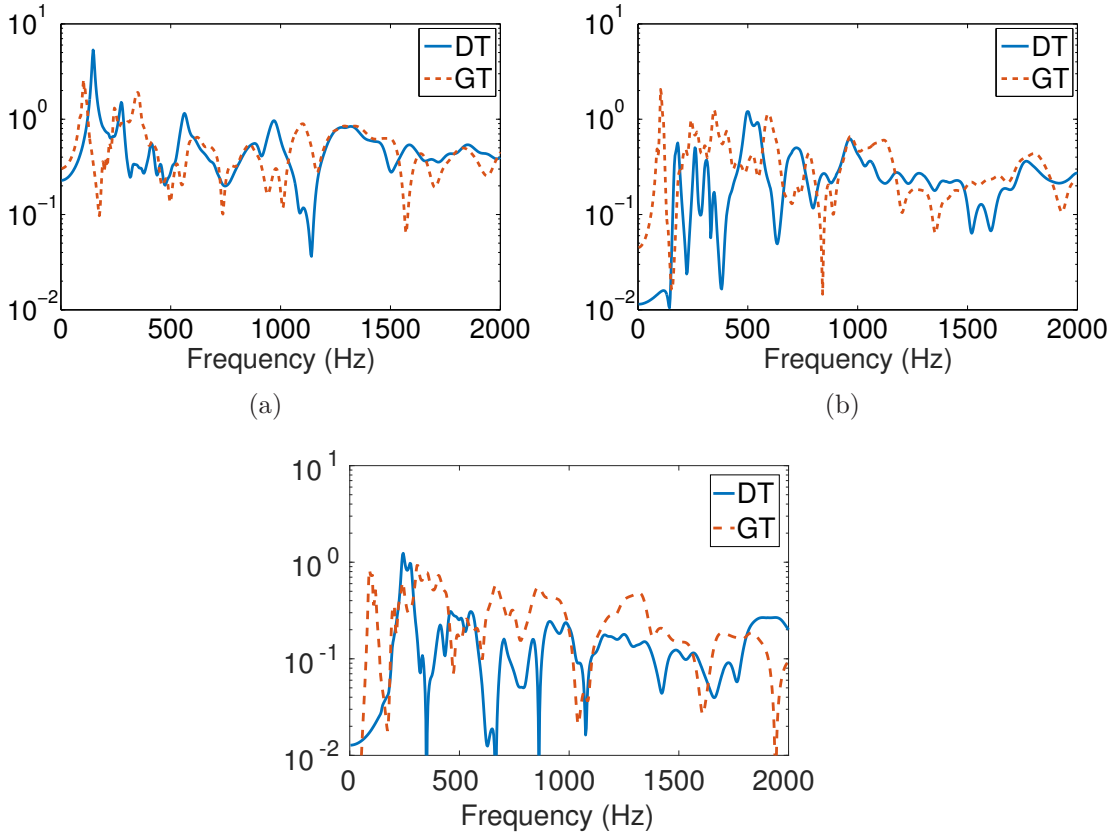


Figure 13: Comparison between the global transfer (GT) and the direct transfer (DT): (a) $\mathbf{T}^D_{1,3}$ and $\mathbf{T}^G_{1,3}$, points located at the same face; (b) $\mathbf{T}^D_{1,5}$ and $\mathbf{T}^G_{1,5}$, points located at adjacent faces; (c) $\mathbf{T}^D_{1,9}$ and $\mathbf{T}^G_{1,9}$, points located at opposite faces. All the curves are FEM simulations.

In that case, all the paths between nodes $i$ and $j$ with $\left|\mathbf{T}^D_{ij}\right|$ which are less than 20% of the maximum coefficient are neglected. The assumption of this 'neglecting criterion' helps in order to clear all the non-meaningful paths and keep only those that are useful in order to characterise the system response. It is also important in order to draw a plot that can be more easily understood. Fig. 14(a) shows a graph map of the most important connections between nodes. In red, the four stronger connections of node 1 are highlighted. The same is done in blue for the three stronger connections of node 4. When identifying these connections in the box geometry (see Fig. 14(b) ), it makes sense. In both cases these connections are the path to the closest nodes. This representation can be different at higher frequencies.

This shows how the outputs provided by ATPA can be represented in a graphic way. The plots help in order to understand the the physical behaviour of the system which is always very important in order to propose an improved design or identify noise and vibration problems.

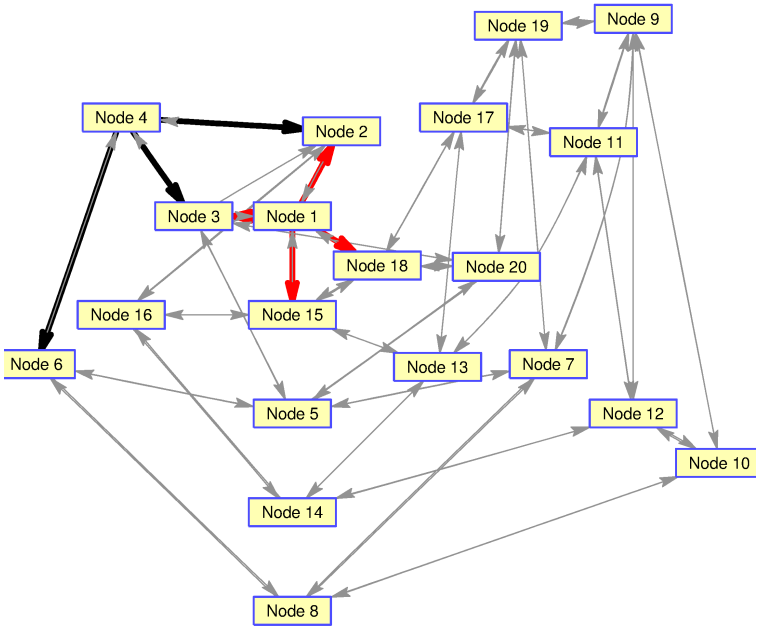


(a)

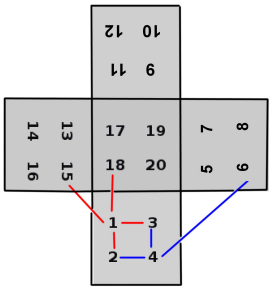


(b)

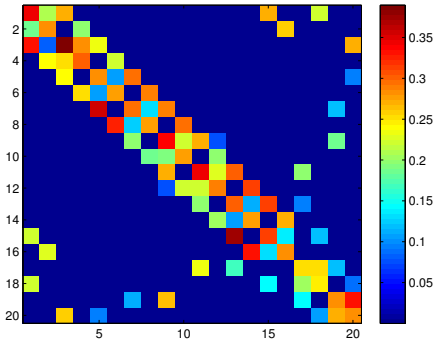


(c)

Figure 14: Graphical representation of the box topology through the direct transfer functions obtained by means of ATPA. Results obtained with the FEM model not considering the air cavity at a frequency of 62.5 Hz: (b) Sketch of the unfolded box where the main transmission paths are highlighted; (a) Graph of the most meaningful connectivities between control points; (c) Colour plot of the direct transfer matrix $\mathbf{T}^D$.

# 4 Conclusions

The main conclusions that can be drawn in view of the results obtained and the experience with the laboratory prototype and the numerical model are as follows:

1. A consistent comparison between the laboratory measurement of a box with air cavity inside and a numerical model of the same box is shown. This validates somehow both the numerical simulations and the reliability of the experimental

measurement. To neglect the radiation losses (effect of the air outside) is a reasonable hypothesis if the interest is focused on the box and air cavity inside. The combination of a multiphysics FEM software (Code Aster [17] with Gmsh [20]) with an automatic pre and post-processing set of scripts is a valid option to reproduce the ATPA procedures.

2. The numerical results show that ATPA procedure is exact if no experimental imprecisions exist. This can be seen with the coincidence of direct transfer functions computed by means of two different procedures in Section 3.1 or the exact reconstruction of the signal for the case of most simple operational excitation shown in Section 3.3.

3. ATPA method properly characterises all the transmission paths, not only the dominant ones.

4. The mechanical connectivity of the system can be defined by means of direct transfer functions. This is frequency-dependent and can be influenced by a proper definition of the measured degrees of freedom and points at the beginning of the process. By taking into account the frequencies that are below the first eigenfrequency, the physical structure of the system is identified.

5. Imprecision in the position where point force is applied has no effect on the outputs at low frequencies but it can be important at mid and high frequencies.

6. The difference between operational and reconstructed signals can be computed a priori. It is the solution of the system excited with operational force and all the control points / degrees of freedom blocked.

7. The type of operational excitation causes some differences in the signal reconstruction. However, they are not very large and can be estimated a priori. The difference is the solution of the problem with the control degrees of freedom blocked and the operational excitation.

# A Calibration of the model and parameter tuning

Two different experimental setups are considered in order to callibrate the model. On the one hand the monitoring of the vibration response of a rectangular plate, see Fig. 15(a). This is used in order to characterise the material properties of the methacrylate. On the other hand, the cuboid-shaped box which is also made of methacrylate with air cavity. This is the mechanical system where ATPA has been applied.

The rectangular plate, with dimensions 0.515 m $\times$ 0.405 m and 8.1 mm thick, is excited by means of a hammer impact at the positions $E_i$ in Fig. 15(b). In every of the realisation of the experiment, with the point force in a different position $E_i$, this input signal (the force measured at the point $E_i$) is denoted by $S_1$. Four accelerometers where the signal $S_i$ $(i = 2, \ldots, 5)$ is measured are distributed judiciously (trying to avoid nodal lines, corners or accelerometers placed close to each other) over the plate.

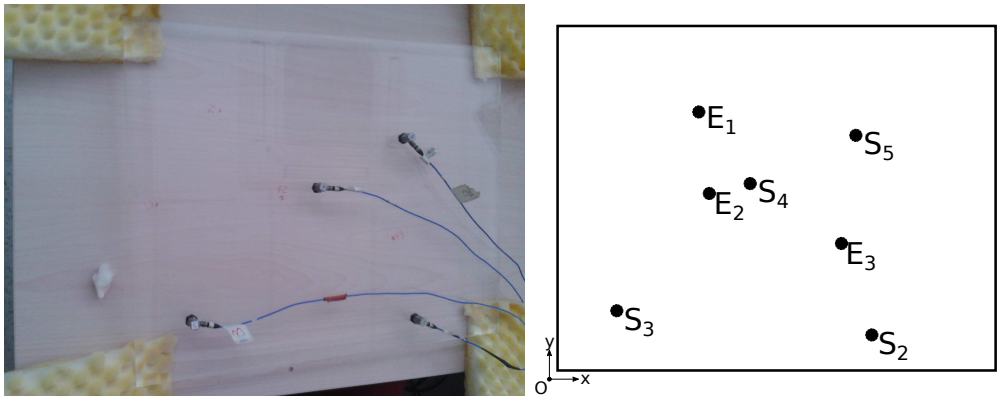


(a) (b)

Figure 15: Rectangular plate: (a) Photo of the instrumented plate; (b) Distribution of the excitation and sensor points in the plate.

| Point | x [m] | y [m] |
|---|---|---|
| $E_1$ | 0.170 | 0.305 |
| $E_2$ | 0.180 | 0.210 |
| $E_3$ | 0.335 | 0.150 |
| $S_2$ | 0.370 | 0.040 |
| $S_3$ | 0.070 | 0.070 |
| $S_4$ | 0.230 | 0.220 |
| $S_5$ | 0.355 | 0.280 |

Table 3: Position of the excitation points $E_i$ and the sensors $S_i$ $(i = 2, \ldots, 5)$ in the plate model.

The positions of excited and control points are listed in Table 3. The plate is supported at the four corners on a very soft foam. Since the stiffness and the mass of the foams is small, the plate is supposed to be tested in free-free conditions. An experimental modal analysis of the plate was done in order to verify this hypothesis. It revealed that the agreement was correct except for the first two modes. For them, the stiffness of the foam had some influence in the response of the plate.

The calibration of the numerical model is done in three stages. First of all, the rectangular plate is used in order to find proper numerical values for the material parameters. It is reasonable to suppose that the methacrylate is a homogeneous and isotropic material. The density is thus obtained from the weight of the plate, see Table 2. The thickness of the plate is approximately constant and the measurements done by means of a calliper were in the range $\pm 0.1$ mm. The details on the determination of the other material parameters are described in Section A.1. Second, the vibration transmission through the corner in an L-shaped junction is measured and compared with the FEM simulation with correct agreement. It was concluded that these glued junctions could be properly modelled as homogeneous junctions. Finally a successful comparison of the box model and the measurements is shown in Section A.2.

| Mode | 1 | 2 | 3 | 4 | 5 | 6 | 7 |
|---|---|---|---|---|---|---|---|
| Eigenfrequency (Hz) | 55 | 61 | 106 | 118 | 137 | 178 | 222 |
| Mode | 8 | 9 | 10 | 11 | 12 | 13 | 14 |
| Eigenfrequency (Hz) | 232 | 286 | 320 | 348 | 362 | 394 | 423 |

Table 4: Eigenfrequencies of the rectangular plate obtained with the experimental modal analysis

## A.1 Material characterization: elasticity modulus and damping

Since the material is supposed to be linearly elastic and the density is known, the required material parameters are the elasticity modulus $E$, the Poisson's ratio $\nu$ and the hysteretic damping $\eta$. $E$ and $\nu$ are supposed to be frequency-independent and $\nu$ is taken from the literature [21, 22]. It is reasonable since $\nu$ does not show a large variation range for this type of material. Once $\nu$ is fixed, the strategy is first to determine $E$ and afterwards adjust a frequency-dependent damping law.

$E$ is chosen in order to fit the first eigenfrequencies in the frequency range with modal behaviour (approximately $100 - 600$ Hz). These eigenfrequencies are obtained from an experimental modal analysis of the plate and can also be identified as the peaks in the experimental curve of Fig. 16. Both eigenfrequency values are very similar and these reference values are listed in Table 4. As commented before, only the two lowest eigenfrequencies are affected by the stiffness of the foam used to sustain the plate.

The experimental curve in Fig. 16 shows the averaged output

$$\psi(f) = \frac{1}{3}\sum_{j=1}^{3}\left|\frac{1}{F_j(f)}\right|\frac{1}{4}\sum_{i=1}^{4}|a_i(f)| \tag{7}$$

where the sum on $i$ is done on all the four sensors of the plate, the sum on $j$ is done on the three impacted positions, $a_i$ and $F_j$ are the phasors of the acceleration and the force registered in the hammer respectively. $\psi$ can be understood as an spatially averaged accelerance. The other curves in Fig. 16 are the results of the equivalent numerical experiments with different values of $E$.

The value of $E$ can differ depending on the methacrylate type. Based on several values published in the literature [21, 22] a variation range is defined and several discrete values of $E$ between 3.0 GPa and 6.0 GPa are considered in order to feed the numerical model and plot curves like the ones in Fig. 16. Each curve has a different peak pattern. It can be seen how the value of $E = 4.3$ GPa fits better the position of the peaks when compared with the experimental measurement. An eigenvalue problem has also been solved in order to verify that the undamped eigenfrequencies are in the same positions as the peaks.

Table 5 shows the arithmetic average of the relative error (considering absolute value in order to avoid sign compensations) between the numerical and experimental eigenfrequencies. The value $E = 4.3$ GPa minimises these differences.

The damping law $\eta(f)$ is chosen in order to minimise the difference in the low frequency peak values (around the eigenfrequencies in the modal response zone) and

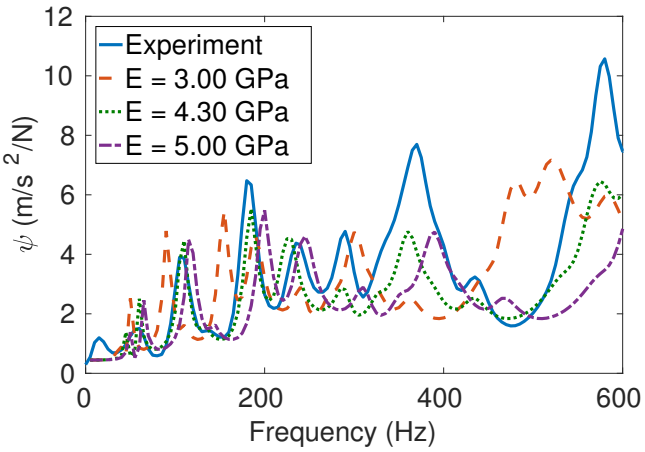


Figure 16: Frequency response function (averaged accelerance $\psi$) for different values of the elasticity modulus. The damping is constant $\eta = 0.07$.

| Elasticity modulus | Mean | Standard deviation |
|---|---|---|
| 3.00 GPa | 17.71% | 4.15% |
| 4.00 GPa | 5.02% | 4.77% |
| 4.30 GPa | 3.04% | 4.18% |
| 4.60 GPa | 4.07% | 3.42% |
| 5.00 GPa | 7.69% | 2.47% |
| 6.00 GPa | 16.59% | 4.97% |

Table 5: Mean relative error of the first 14 eigenfrequencies depending on the value of $E$. The results of the experimental modal analysis are taken as a reference.

also to properly reproduce the trend at high frequencies. Fig. 17 shows some of the damping laws with the form $\eta = a + \omega^b$, where $a$ and $b$ are constants to fit. A minimisation of the difference between the computed and experimental curve in the whole frequency range (not only at the eigenfrequencies) leads to the following expression of the damping

$$\eta = 0.07 + \frac{1}{\omega} \tag{8}$$

## A.2 Box model validation

Once the material parameters of the methacrylate are calibrated by means of the rectangular plate experiment, the response provided by the numerical model of the box is compared with measured data. The problem is vibroacoustic, including the cavity inside the box. The air parameters for the numerical model are taken from the literature: sound velocity in air $c = 345.23$ m/s and air density $\rho_a = 1.18$ kg/m$^3$.

A shaker is installed in the position of accelerometer ACC6, see Fig. 3. This allows a better control of the position where the excitation is applied. The shaker is fixed to the face and the uncertainty of human manipulation of the hammer impact is suppressed. The output defined in Eq. (7) is considered for comparison. $\psi$ is computed

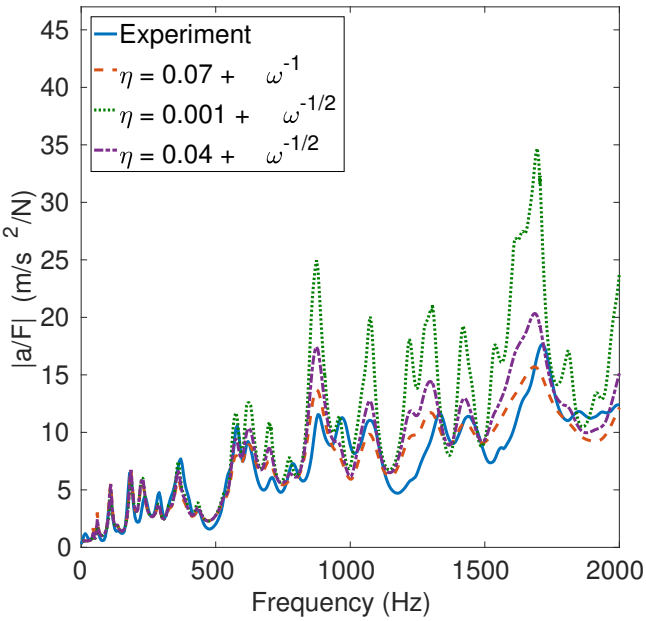


Figure 17: Frequency response function (accelerance) between two arbitrary points with three different values of the damping coefficient. According to the notation $\eta = a + \omega^b$: $(a = 0.07, b = -1)$, $(a = 0.001, b = -1/2)$ and $(a = 0.04, b = -1/2)$.

| Plate | $e$ |
|---|---|
| Top | 14.12% |
| Front | 18.82% |
| Back | 8.40% |
| Left | 8.89% |
| Right | 6.21% |

Table 6: Difference between the experimental measurement and the simulation in each face of the plate according to Eq. (6).

at every plate taking into account the four accelerometers, with the difference that only one force position is considered (where the shaker is placed). Fig. 18 shows the parameter $\psi$ for the top plate. The agreement is very good in both the shape of the curve and also the magnitude. We have not absolute certainty for the experimental measurements below 100 Hz. The reasons are several as exposed above: difficulty in the proper excitation of rigid-body motion modes and interference with the background noise/vibration. Similar results are obtained for the other faces of the box. A global measure of the error is shown in Table 6 where the difference between frequency response curves is measured by means of Eq. (6).

Fig. 19 shows the comparison for the averaged square pressure at the microphones placed inside the cavity. The measure of the difference between experimental and numerical curves is 7.25%. The agreement is deemed sufficient.

The global agreement between the numerical results and the experimental measurements is good both in terms of vibration and acoustic pressure. Moreover, the

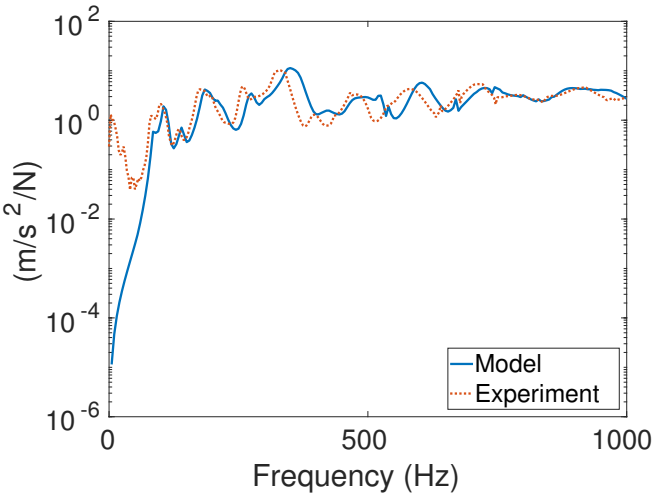


Figure 18: Comparison between the experiment and the numerical simulation. $\psi_{\text{exp}}$ and $\psi_{\text{FEM}}$ curves at the top plate due to the action of the shaker in the position ACC6.

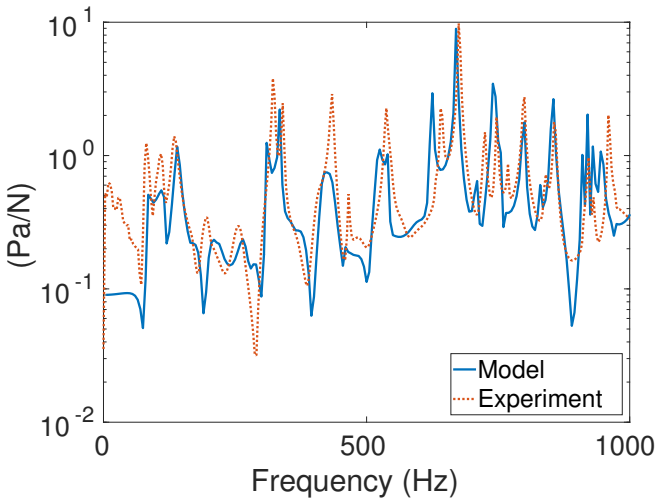


Figure 19: Absolute value of the averaged square pressure divided by the point force $|p/F|$ at the micros inside the cavity due to the action of the shaker in the position ACC6. Comparison between the experiment and the numerical simulation.

usual outputs of interest and regulation parameters are presented in dB. This means that the relevance of these differences from the engineering point of view is of less importance. It is also true that the chosen parameters are somehow spatially averaged (few positions are considered). When outputs in a specific position are regarded, the differences are expected to be a bit larger due to the spatial shift of the pressure and vibration waves.

# Acknowledgements

The authors would like to thank Clement Dalmagne (ICR) for his collaboration with the experimental measurements. This research is supported by the project 'Nous horitzonts pels outputs de l'ATPA (NHOA, RD15-1-0083)' which is founded by ACCIO of the Generalitat de Catalunya in the framework of the FEDER Catalunya 2014-20120 operative program. LaCàN research group is grateful for the sponsorship/funding received from Generalitat de Catalunya (Grant number 2017-SGR-1278).


# References


[1] F. X. Magrans. Method of measuring transmission paths. *J. Sound Vibr.*, 74(3):321–330, 1981.

[2] F. X. Magrans, J. Poblet-Puig, and A. Rodríguez-Ferran. A subsystem identification method based on the path concept with coupling strength estimation. *Mech. Syst. Signal Proc.*, 100(Supplement C):588–604, 2018.

[3] M. Van Der Seijs, D. de Klerk, and D. J. Rixen. General framework for transfer path analysis: History, theory and classification of techniques. *Mech. Syst. Signal Proc.*, (68–69):217–244, 2015.

[4] S. A. Hambric, S. H. Sung, and D. J. Nefske. *Engineering Vibroacoustic Analysis: Methods and Applications*. John Wiley & Sons, 2016.

[5] F. X. Magrans, P. V. Rodríguez, and G. C. Cousin. Low and mid-high frequency advanced transmission path analysis. In *Proceedings of the Twelfth International Congress on Sound and Vibration ICSV12*, 2005.

[6] O. Guasch, C. García, J. Jové, and P. Artís. Experimental validation of the direct transmissibility approach to classical transfer path analysis on a mechanical setup. *Mech. Syst. Signal Proc.*, 37(1):353–369, 2013.

[7] N. Zafeiropoulos, A. T. Moorhouse, A. Mackay, and U. Senapati. Advanced transfer path analysis of a vehicle. In *Proceedings of the 11 RASD conference, Pisa*, 2013.

[8] A.T. Moorhouse, A.S. Elliott, and T.A. Evans. In situ measurement of the blocked force of structure-borne sound sources. *J. Sound Vibr.*, 325(4-5):679–685, 2009.

[9] N. Patil and A. Moorhouse. Applications of the in-situ airborne transfer path analysis (tpa) technique in the diagnosis of sound transmission paths of a building element. In *INTER-NOISE and NOISE-CON Congress and Conference Proceedings*, volume 253, pages 6657–6666. Institute of Noise Control Engineering, 2016.

[10] O. Guasch. Direct transfer functions and path blocking in a discrete mechanical system. *J. Sound Vibr.*, 321(3):854–874, 2009.

[11] N. B. Roozen and Q. Leclere. On the use of artificial excitation in operational transfer path analysis. *Applied Acoustics*, 74(10):1167–1174, 2013.

[12] N. Totaro and J.L. Guyader. SEA substructuring using cluster analysis: The MIR index. *J. Sound Vibr.*, 290(1-2):264–289, 2006.

[13] C. Díaz-Cereceda, J. Poblet-Puig, and A. Rodríguez-Ferran. Automatic subsystem identification in statistical energy analysis. *Mech. Syst. Signal Proc.*, 54-55:182–194, 2015.

[14] Francesc Xavier Magrans, Jordi Poblet-Puig, and Antonio Rodríguez-Ferran. A subsystem identification method based on the path concept with coupling strength estimation. *Mech. Syst. Signal Proc.*, 100:588–604, 2018.

[15] Y. Lebresne. Interventions practiques contre les bruits exterieurs des vehicles routiers. In *Conferences Interkeller Gap (Zurich)*, number 11, pages 1–36, 1975.

[16] F. X. Magrans, J. Poblet-Puig, and A. Rodríguez-Ferran. The solution of linear mechanical systems in terms of path superposition. *Mech. Syst. Signal Proc.*, 85:111–125, 2017.

[17] EDF. Code-Aster home page. http://www.code-aster.org, 2017.

[18] J-. L. Batoz, K-. J. Bathe, and L-. W. Ho. A study of three-node triangular plate bending elements. *International Journal for Numerical Methods in Engineering*, 15(12):1771–1812, 1980.

[19] O. Guasch and F. X. Magrans. The global transfer direct transfer method applied to a finite simply supported elastic beam. *J. Sound Vibr.*, 276(12):335–359, 2004.

[20] C. Geuzaine and J.-F. Remacle. Gmsh: a three-dimensional finite element mesh generator with built-in pre- and post-processing facilities. *Int. J. Numer. Meth. Engng.*, 11(79):1309–1331, 2009.

[21] B. Bhushan and Z. Burton. Adhesion and friction properties of polymers in microfluidic devices. *Nanotechnology*, 16(4):467, 2005.

[22] G. Wei, B. Bhushan, N. Ferrell, and D. Hansford. Microfabrication and nanomechanical characterization of polymer microelectromechanical system for biological applications. *Journal of Vacuum Science & Technology A: Vacuum, Surfaces, and Films*, 23(4):811–819, 2005.